Climate change influences chlorophylls and bacteriochlorophylls metabolism in hypersaline microbial mat

Camille Mazière, M. Bodo, M.A. Perdrau, Cristiana Cravo-Laureau, Robert Duran, C. Dupuy, Cédric Hubas

▶ **To cite this version:**

Camille Mazière, M. Bodo, M.A. Perdrau, Cristiana Cravo-Laureau, Robert Duran, et al.. Climate change influences chlorophylls and bacteriochlorophylls metabolism in hypersaline microbial mat. Science of the Total Environment, 2022, 802, pp.149787. 10.1016/j.scitotenv.2021.149787 . hal-03328597

HAL Id: hal-03328597
https://hal.science/hal-03328597v1

Submitted on 28 Jun 2023

HAL is a multi-disciplinary open access archive for the deposit and dissemination of scientific research documents, whether they are published or not. The documents may come from teaching and research institutions in France or abroad, or from public or private research centers.

L'archive ouverte pluridisciplinaire **HAL**, est destinée au dépôt et à la diffusion de documents scientifiques de niveau recherche, publiés ou non, émanant des établissements d'enseignement et de recherche français ou étrangers, des laboratoires publics ou privés.

Version of Record: https://www.sciencedirect.com/science/article/pii/S0048969721048622
Manuscript_90128dbc8cc37a45d126edb6d2d70bf3

Climate change influences chlorophylls and bacteriochlorophylls metabolism in hypersaline microbial mat

C. Mazière[1,2*], M. Bodo[3], M. A. Perdrau[2], C. Cravo-Laureau[1], R. Duran[1], C. Dupuy[2], C. Hubas[3]

[1] Université de Pau et des Pays de l'Adour, E2S UPPA, CNRS, IPREM UMR 525 - Bât. IBEAS, BP1155, 64013 PAU cedex, France

[2] La Rochelle Université, CNRS, UMR 7266 LIENSs (Littoral Environnement et Sociétés)- 2, rue Olympe de Gouges, Bât. ILE, 17000 LA ROCHELLE, France

[3] Muséum National d'Histoire Naturelle, UMR BOREA 8067, MNHN-IRD-CNRS-SU-UCN-UA - Station Marine de Concarneau, 29900 CONCARNEAU, France

* Corresponding author: camille.maziere@univ-pau.fr, +33 5 59 40 74 68, Bâtiment IBEAS – avenue de l'Université – 64013 Pau, France ; +33 5 46 50 76 31, Bâtiment Ile – 2, rue Olympe de Gouges – 17000 La Rochelle, France

Keywords: hypersaline microbial mats, ocean acidification, mesocosms, chlorophyll derivatives, phototrophic communities

Abstract

This study aimed to determine the effect of the climatic change on the phototrophic communities of hypersaline microbial mats. Ocean acidification and warming were simulated alone and together on microbial mats placed into mesocosms. As expected, the temperature in the warming treatments increased by 4°C from the initial temperature. Surprisingly, no significance difference was observed between the water pH of the different treatments despite of a decrease of 0.4 unit pH in the water reserves of acidification treatments. The salinity increased on the warming treatments and the dissolved oxygen concentration increased and was higher on the acidification treatments. A total of 37 pigments were

© 2021 published by Elsevier. This manuscript is made available under the Elsevier user license
https://www.elsevier.com/open-access/userlicense/1.0/

identified belonging to chlorophylls, carotenes and xanthophylls families. The higher abundance of unknown chlorophyll molecules called chlorophyll derivatives was observed in the acidification alone treatment with a decrease in chlorophyll *a* abundance. This change in pigmentary composition was accompanied by a higher production of bound extracellular carbohydrates but didn't affect the photosynthetic efficiency of the microbial mats. A careful analysis of the absorption properties of these molecules indicated that these chlorophyll derivatives were likely bacteriochlorophyll *c* contained in the chlorosomes of green anoxygenic phototroph bacteria. Two hypotheses can be drawn from these results: 1/ the phototrophic communities of the microbial mats were modified under acidification treatment leading to a higher relative abundance of green anoxygenic bacteria, or 2/ the highest availability of CO_2 in the environment has led to a shift in the metabolism of green anoxygenic bacteria being more competitive than other phototrophs.

1. Introduction

Since the industrial revolution, the atmospheric greenhouse gases concentration has increased sharply leading to a decrease in the pH of the surface ocean of about 0.1 pH unit (IPCC, 2014). In the coming decades, the ocean acidification will continue, associated with an ocean water warming caused by increasing levels of CO_2 in the atmosphere (Hutchins and Fu, 2017; IPCC, 2014). These climatic perturbations will alter the carbon and nutrients cycles on a global scale (Hutchins and Fu, 2017) and are expected to have a direct impact on all physical, chemical and biological parameters that govern marine organisms life (Hutchins and Fu, 2017). Organisms will be faced with unprecedented changes in future ocean conditions, particularly marine life will be severely affected. On France's Atlantic coasts, the Intergovernmental Panel on Climate Change (IPCC) predicts an increase in surface water temperature of 3 to 4 °C and ocean acidification of 0.4 to 0.45 pH units in its most pessimistic scenario (RCP 8.5) by the end of the century (IPCC, 2014).

Research on microorganisms facing climatic changes is scarce compared to that on animals and plants (Cavicchioli et al., 2019; Dutta and Dutta, 2016; Reinold et al., 2019). Microbial mats play important key-roles in marine ecosystems, such as participating in the dynamics of carbon, nitrogen et oxygen cycles. They develop at the water-sediment interface in a large variety of environments including coastal beaches (Bolhuis and Stal, 2011), salterns (Fourçans et al., 2004), hot springs (Dobretsov et al., 2011) and many other coastal/marine environments. These are complex microbial structures containing a great diversity of microorganisms coexisting at microscale according to a vertical stratification due to light and microgradients of oxygen, pH and sulphurs (Fourçans et al., 2008; Jorgensen et al., 1983; Revsbech et al., 1983; van Gemerden, 1993). Despite the stratification, microbial mats are dynamic structures where the migration of microorganisms has been described according to the diel cycle (Fourçans et al., 2008, 2006). Numerous interactions occurs in microbial mats representing thus an ecosystem on its own (Reinold et al., 2019). Microbial mats have a remarkable specific, metabolic and molecular diversity, making them highly adaptable to the changing physico-chemical conditions of the environment (Fourçans et al., 2006) as well as to contamination (Bordenave et al., 2008, 2004a, 2004b).

microorganisms are fundamental organisms in the functioning of microbial mats because they are primary producers.

Autotrophic microorganisms are fundamental organisms in the functioning of microbial mats because they are the major primary producers. They can be chemotroph such as some Bacteroidetes but the major primary producers in photosynthetic microbial mats are the phototrophic microorganisms (Sørensen et al., 2005). Among them, Cyanobacteria produce organic carbon which is then decomposed in the successive lower layers by different heterotrophs. They also secrete adhesive and protective extracellular polymeric substances (EPS), that form a matrix around the cells (Decho, 1990; Fourçans et al., 2006; Hubas, 2018; Wieland et al., 2003). This matrix is generally composed of sugars, proteins, extracellular DNA and other molecules in smaller proportions (Fourçans et al., 2006; Hubas, 2018;

87 Wieland et al., 2003). However, the composition varies depending on the physiological state
88 of the organisms, the specific diversity, the growth stage of the mat and the physico-chemical
89 conditions of the environment (Decho and Moriarty, 1990; Hubas, 2018; Reinold et al., 2019;
90 Underwood et al., 2004). By binding to sedimentary particles, this matrix stabilises the
91 microbial mat and prevents erosion phenomena (Decho, 1990), but it has many other
92 essential roles such as nutrients supply by the sequestration and accumulation of dissolved
93 and particulate nutrients coming from the water column that can be used by microorganisms,
94 or it also helps microbial communication, or bring a protection against UV radiations (Decho,
95 2000; Flemming and Wingender, 2010; Hubas, 2018). EPS are therefore a major component
96 of microbial mats and remain indispensable for their functioning.

97 Several studies have addressed the impact of climate change on photosynthetic marine
98 microbial communities. Some authors have shown that temperature affects the composition,
99 the photosynthetic performance as well as the growth, biomass and physiology of
100 microphytobenthos (Cartaxana et al., 2015; Hancke and Glud, 2004). Acidification effects are
101 thought to occur mainly at the metabolic level, favouring the growth of some microorganisms
102 (Baragi and Anil, 2016; Black et al., 2019; Hicks et al., 2011) but also photorespiration in
103 diatoms and increasing the number of proton pumps for maintaining intracellular pH
104 homeostasis and respiratory processes (Beardall et al., 2009; Black et al., 2019; Gao et al.,
105 2012). Acidification and warming also affect the characteristics of EPS of diatoms and
106 cyanobacteria with a modification of their composition (Li et al., 2016; Ma et al., 2019).

107 Many studies have highlighted the impact of acidification and warming water separately but it
108 is necessary to consider them together as they can act synergistically (Baragi et al., 2015;
109 Baragi and Anil, 2016; Li et al., 2016). The aim of this study was to simulate an acidification
110 and a water warming on microbial mats on mesocosms according to the RCP8.5 scenario of
111 the IPPC for 2100. Here, the phototrophic microbial communities are described and their
112 potential composition variation will be monitored.

113

2. Material and methods

2.1 Description of the sampled sites

Microbial mats for mesocosms experiment were sampled the 30th April 2019 in salterns located in Ars-en-Ré (46°13'29.9"N 1°31'07.5"W, Ré island, France) on a non-exploited pond. The microbial mat, which had not been disturbed for at least three years, was more mature than a mat from an exploited pond. Undisturbed mats were then placed in plastic boxes and transported to laboratory at room temperature where they were put back in water within three hours following the sampling. The water height was around 3 cm as observed *in situ*. *In situ* physico-chemical parameters (temperature, salinity, pH) of the water were measured with a multi-parameter probe (pHenomenal® MU 6100H, VWRTM, USA) in order to apply them on the mesocosms as control values. Samples were also taken to determine nutrient salt concentrations in the pore water.

2.2 Mesocosm design

Microbial mats were separated into twenty-four plastic boxes (48 cm x 33 cm), each of them representing a mesocosm (Fig. 1). The mesocosms were gathered in groups of six representing a condition (five replicates and a box for pulse amplitude modulated (PAM) measures). In these six mesocosms, incoming water was from a reserve and was distributed individually with stainless steel taps. This water corresponded to seawater filtered at 80 µm, passed under UV light and whose salinity was adjusted to 60 psu with salt coming the salt marshes of the Ré island. Opposite to the water inlet, a hole allowed the water outlet in a network of PVC tubes between all the replicates. The water was not recycled. This setup permitted to maintain a stable water level at 3 cm above the mat and to renew seawater and the supplying nutrients for the development of the microbial mats. For each condition, a pool was constructed around the six plastic boxes where water was maintained at the desired temperature with a pump (EHEIM universal 600, Germany) connected to a thermoregulating

device (Teco®) to control the water temperature above the microbial mats. The microbial mats were illuminated twelve hours a day following the day/night cycle observed during the spring. To control the evaporation rate, the lights used were LED (TOP-24H company by SYLED, France). They provided white cold light color and an intensity of 11.8 ± 0.9 µmol.photons.m^{-2}.s^{-1} (mean ± standard between the four treatments for a day) (HOBO Pendant® Temperature/Light Data Logger, Onset Computer Corporation, USA) on the surface of the microbial mats.

Daily monitoring was done for the physico-chemical parameters (temperature, pH, salinity and dissolved oxygen) thanks to a multiparameter probe (pHenomenal® MU 6100H, VWR™, USA).

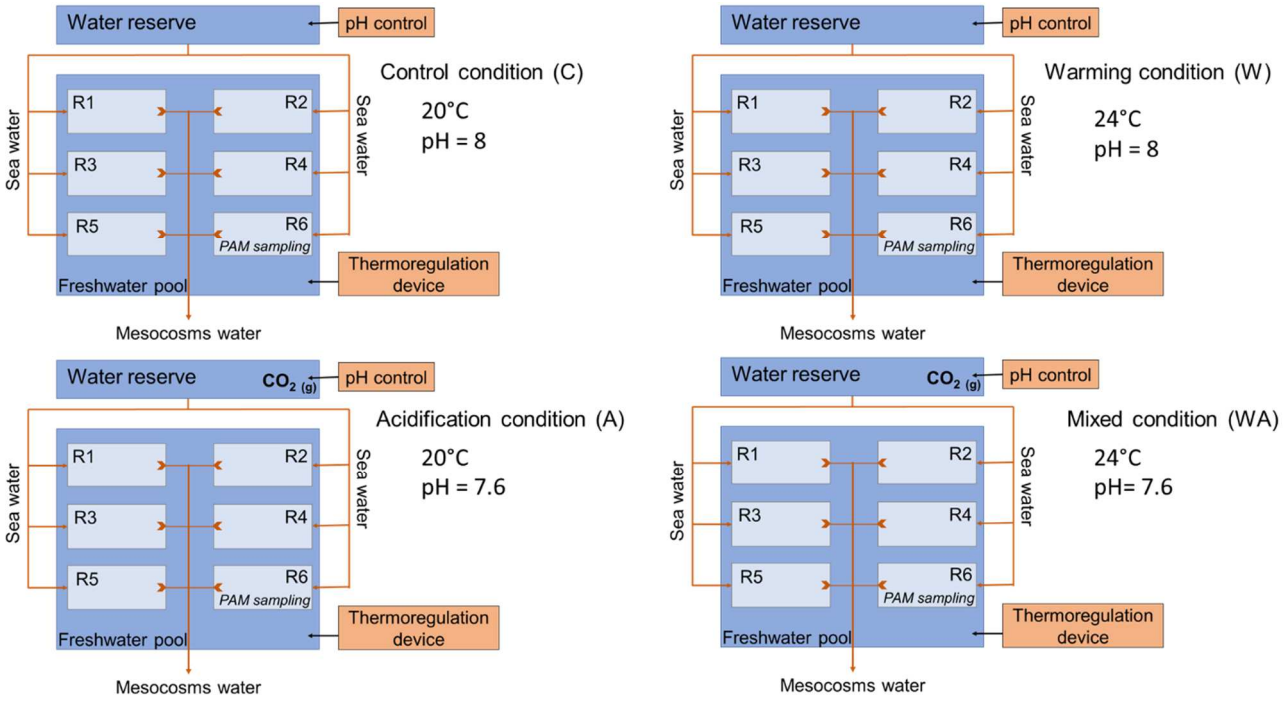

Figure 1: Schematic representation of the experimental device with the control (C) and the acidification (A), warming (W) and mixed (WA) treatments. The replicates are represented by the letter R, the first five are used for sampling and the sixth is dedicated to the measurements of fluorimetry by pulse amplitude modulation (PAM).

2.3 Implementation of different treatments

A stabilisation period of five weeks was applied to acclimate the microbial mats to their new environment (Gette-Bouvarot et al., 2015; Stauffert et al., 2013). The water temperature on

the mesocosms was maintained at 20°C and the salinity of the incoming water was regulated in the water reserve to maintain a salinity at 60 +/- 2 psu in the mesocosms, reproducing *in situ* conditions. The implementation of different treatments occurred for seven additional weeks.

Four treatments were applied to the microbial mats. Each pool and its six mesocosms represented a condition. The first treatment was the control treatment (C) in which the parameters were not changed. The second treatment was the warming treatment (W) in which the temperature was increased by 0.5°C every two days for 2 weeks until reaching 24°C. The acidification treatment (A) represented the third condition. The water acidification was performed in the water reserve by bubbling pure CO_2, allowing a drop of initial water pH of 0.1 unit every four days for 2 weeks until reaching a decrease of the initial pH of the water reserve equal to 0.4 unit, *i.e.* 7.6. The water pH in the water reserve was monitored with a continuous pH stat system (IKS aquastar**,** iks ComputerSysteme GmbH, Germany). Then the pH values of the pH stat system were adjusted twice a week from measurement using a pH meter (Metrohm, 826 pH mobile) with a glass electrode (Metrohm, electrode plus) calibrated on the total scale using Tris buffer solution (provided by Andrew Dickson, Scripps Institution Oceanography, San Diego). Every day, the pH values in the four treatments pools were also measured on the total scale. The fourth treatment combined warming and acidification treatments (WA). The mesocosms were then maintained under these treatments for 5 further weeks.

A first sampling (noted t9) was performed after the stabilisation period of the microbial mats on the mesocosms, just before changing the environmental conditions. A second sampling (t16) was performed at the middle of the period of change and a third (t23) at the end (Supplementary materials, fig. A). After this period, sampling was performed every week (t30, t37, t44, t51 and t58) (Supplementary materials, fig. A). For each sampling, ten 1 cm depth cores were collected with a 1 cm diameter cut-off syringe in each mesocosm and mixed together in order to obtain a homogeneous sample.

2.4 Nutrient concentrations

A volume of 20 mL of water from each mesocosm was filtered at 0.22 µm in order to perform a nutrient analysis. The same was done for *in situ* samples. Half of the volume was frozen at -20°C while the other half was kept at 4°C for silicon analysis. The samples were then analyzed as described by Aminot and Kérouel (2007). Silicon, nitrate, nitrite and phosphate were measured by Segmented Continuous Flow Colorimetry (SFA) while ammonium was measured by SFA fluorimetry on an auto-analyser (SEAL AutoAnalyzer 3, SEAL analytical) (Aminot and Kérouel, 2007).

2.5 Photosynthetic parameters

Chlorophyll fluorescence parameters were measured at 5 different locations of the core using a fluorometer (Monitoring Pen, MP 100-E, Photon Systems Instruments, Czech Republic) illuminated with a blue LED emitter (455 nm). The samples were placed in the dark (for 5 min) before the measurement of Light Response Curves. Manufacturer predetermined LC3 protocol was used following manufacturer instructions. LC3 protocol was characterised by 7 steps of increasing light intensities (10, 20, 50, 100, 300, 500, 1000 µmol.photon.m^{-2}.s^{-1}) with an illumination duration of 60s. Minimum fluorescence level F_0[5] (Jesus et al., 2006) was obtained by using a non actinic measuring light pulse (30 µs, 900 µmol.photon.m^{-2}.s^{-1}), which induced the minimal chlorophyll fluorescence (F_0[5]).The samples were then subjected to a saturating light pulse (2,400 µmol.photon.m^{-2}.s^{-1}). This made it possible to measure the maximum fluorescence level F_m[5] (Jesus et al., 2006). All measurement were done in the same conditions and at the same time.

The data was then downloaded from the device to a computer using FluorPen software (v1.0.6.1, Photon Systems Instruments, Czech Republic) and all calculations and analyses were performed using R.Studio software (version 4.0.3© RStudio, Inc.). From the measured parameters the effective quantum yields of photosynthesis ($\phi(II)$[5]) were calculated (Jesus et

al., 2006) (Equation 1). They indicate the community's maximum potential for photosynthetic activity.

$$\phi(II)^5 = \frac{F_m{}^5 - F_0{}^5}{F_m{}^5} \quad \text{(Equation 1)}$$

2.6 Pigment identification and quantification

Lipophilic pigments were analyzed by high performance liquid chromatography (HPLC). Microbial mats were incubated with 95% methanol (buffered with 2% ammonium acetate) during 15 min, at -20°C in the dark. Extracts were then filtered with 0.2µm PTFE syringe filters and analyzed within 16h using an Agilent 1260 Infinity HPLC composed of a quaternary pump (VL 400 bar), a UV–VIS photodiode array detector (DAD 1260 VL, 190–950 nm), a fluorescence detector (FLD 1260 excitation: 425 nm, emission: 655 nm), and a 100µl automatic sample injector refrigerated at 4°C in the dark. Chromatographic separation was carried out using a C18 column for reverse phase chromatography (Supelcosil, 25 cm long, 4.6 mm inner diameter). The solvents used were: 0.5M ammonium acetate in methanol and water (85:15, v:v), acetonitrile and water (90:10, v:v), and 100% ethyl acetate. The solvent gradient was set according to Brotas and Plante-Cuny (2003), with a 0.5 mL min−1 flow rate. Identification and calibration of the HPLC peaks were performed with *ββ*-carotene, canthaxanthin, chlorophyll *a*, chlorophyll *b*, chlorophyll *c2*, diatoxanthin, diadinoxanthin, fucoxanthin and pheophytin *a* standards. We identified all detected peaks by their absorption spectra and relative retention times using the Agilent OpenLab software. Quantification was performed using standard calibration curves built with repeated injections of standards over a range of dilutions. Xanthophylls, carotens and chlorophyll b and c were quantified at 470 nm, chlorophyll *a* and their derivatives as well as pheopigments were quantified at 665 nm. The relative abundance of each pigment (%) was calculated from its respective concentration in the sample (µg.mg^{-1}).

2.7 Extracellular Polymeric Substances (EPS) characterization

In a 15 mL Falcon® tube, 5 mL of microbial mat was mixed with an equivalent volume of seawater obtained by mixing water from the five sampled replicate and filtered at 0.22 µm for each treatment. The tubes were subjected to mechanical agitation by vortexing and by inversion at a rate of 40 oscillations.min^{-1} for 1 h at 4°C in the dark. Then they were centrifuged at 3500 g for 10 min at 4°C. The supernatant, containing the colloidal fraction, was recovered and stored at -20°C while the pellet, containing the bound fraction, was resuspended in 5 mL of seawater (again obtained by mixing water from the five sampled replicate and filtered at 0.22 µm for each treatment). 1 g of Dowex resin (Dowex Marathon C, Na^+, Sigma-Aldrich), was prepared according to the protocol of Takahashi *et al.* (2009). The tubes were again subjected to the same protocol to obtain the supernatant containing the fraction of bound EPS was recovered and stored at -20°C.

The carbohydrate dosage was performed according to Dubois' colorimetric method(Dubois et al., 1956) while the protein dosage was performed according to the BiCinchoninic acid Assay (BCA) method using the Pierce™ Protein Assay Kit (Thermoscientific). A range of glucose (L-(-)-Glucose, 98%, Sigma-Aldrich) from 0 to 3 g.L^{-1} and a range of bovine serum albumin (BSA) from 0 to 1 g.L^{-1} were performed in seawater from the Ré island hypersalinated at 60 psu and filtered at 0.22 µm. For carbohydrates, 100 µL of EPS sample were placed in a tube, then 100 µL of 5% phenol (Solid Phenol, Sigma-Aldrich, France) and 500 µL of 98% sulphuric acid (Sulphuric Acid 98%, Carlo-Erba Reagents, France) were added. The tubes were incubated for 30 min in the dark and at room temperature. A volume of 200 µL of the standard range and each triplicate sample was deposited in a 96-well microplate (Falcon® 96-well Clear Microplat, Thermo Fisher Scientific). The absorbance of each well was measured at 490 nm with a spectrophotometer (SPECTROstar® Nano, BMG LAB). For proteins, 225 mL of reagent was prepared and stored in the dark at room temperature during the assay period. The assays were performed in 96-well microplates (Falcon® 96-well Clear Microplat, Thermo Fisher Scientific). 200 µL of reagents were placed in the wells and 25 µL standards or

triplicate samples were added. The microplates were incubated for 30 min at 37°C, then the absorbance of each sample was measured at 562 nm by a spectrophotometer (SPECTROstar® Nano, BMG LAB). Two calibration curves were drawn from the standard ranges and their respective abundances (corrected according to the kit indications for the BSA range), averaged over the duration of the experiment. They made it possible to determine the carbohydrate and protein concentrations. The latter were then related to the dry mass of the microbial mat.

To determine the dry mass of the microbial mat, a volume of 30 mL of microbial mat was collected and weighed to obtain the fresh mass (M_F). The sample was then freeze-dried to remove water from the sample (Lyophilisateur Christ Alpha 1-4, Grosseron, France) and re-weighed to obtain the freeze-dried mass (M_L).

2.8 Data analysis

All calculations and analyses were performed on R.Studio software (version 4.0.3© RStudio, Inc.). The mean of physico-chemical parameters, the carbohydrates and proteins concentrations of each fraction and the photosynthetic parameters of each treatment were compared with each other at each sampling time. The normality and homoscedasticity of the data were previously verified by carrying out a Shapiro test and a Bartlett test respectively. If both conditions were met, the data were subjected to an analysis of variances (ANOVA). Otherwise, a Welch ANOVA was performed in the case of non-homogeneity of variances and a Kruskal-Wallis rank sum test in the case of non-normal data. If these tests were found to be significant ($p < 0.05$), then a pairwise comparison was performed using a Tukey test following the ANOVA, a Games-Howell test following a Welch ANOVA or a Nemenyi test following the Kruskal-Wallis test.

A Between Class Analysis (BCA) combined with hierarchical cluster analysis with a Bray dissimilarity index and ward.D2 method was done on pigments proportions.

3. Results

3.1 Efficiency of the physico-chemical changes

As expected, the temperature in W and WA treatments increased well by 4°C from the initial temperature, the one maintained in C and A treatments (23.89 ± 0.49°C; 23.82 ± 0.48°C; 20.32 ± 0.36°C; 20.23 ± 0.48°C; respectively) (Fig. 2, A; Supplementary materials, fig. B). There was a delay of one week before reaching this increase after the change of state because this was the time needed to heat up all the water in the pool and then the mesocosms.

The pH of C and W treatments were stabilized after t37 at 7.94 ± 0.15 and 7.95 ± 0.09, respectively (Fig.2, B; Supplementary materials, fig. B). The pH of A and WA treatments decreased until t44, then remaining stable at pH 7.87 ± 0.13 and 7.86 ± 0.10, respectively (Fig.2, B; Supplementary materials, fig. B). No significant difference between the four treatments was found at t9 (Kruskal, $p > 0.05$).

The salinity (Fig. 2, C; Supplementary materials, fig. B) of C and A treatments remained stable at 60.87 ± 1.44 psu and 61.91 ± 1.79 psu, respectively. The salinity of the W treatment increased to a maximum mean value of 75.87 ± 4.84 psu after 40 days of incubation, and then decreased again to a final value of 67.35 ± 4.24 psu. The salinity of the WA treatment increased and reached its maximum value of 71.94 ± 6.55 psu on day 23 of the experiment and then decreased and remained at 66.13 ± 2.56 psu.

Dissolved oxygen remained stable between each treatment up to t16 (mean ± standard deviation; 0.95 ± 1.18 $mg.L^{-1}$ for control, 0.61 ± 1.15 $mg.L^{-1}$ for pH, 0.60 ± 0.46 $mg.L^{-1}$ for W and 0.30 ± 0.24 $mg.L^{-1}$ for WA) (Fig. 2, D; Supplementary materials, fig. B). From t23, the dissolved oxygen of the treatments increased linearly to t58 with a slope of 0.07 day^{-1} (R^2 = 0.45, Student-test, $p < 0.05$) for A, 0.05 day^{-1} (R^2 = 0.39, Student-test, $p < 0.05$) for W and 0.03 day^{-1} (R^2 = 0.19, Student-test, $p < 0.05$) for WA. The A treatment had a final oxygen concentration of 5.95 ± 1.63 $mg.L^{-1}$, significantly higher (ANOVA, $p < 0.05$) than that of the

other mesocosms by a factor of 1.6 for W, 2.2 for C and 2.4 for WA (mean ± standard deviation).

The nutrients were analyzed thanks to the Redfield ratio calculations (Redfield, 1958). Only seven samples showed nitrogen limitation, notably four replicates of the A treatment at t30 and some samples showed a limitation of silicon (Supplementary materials, fig. B and C). Most of the samples showed phosphate limitation, but such phosphate limitation was also observed *in situ* (Supplementary materials, fig. B and C).

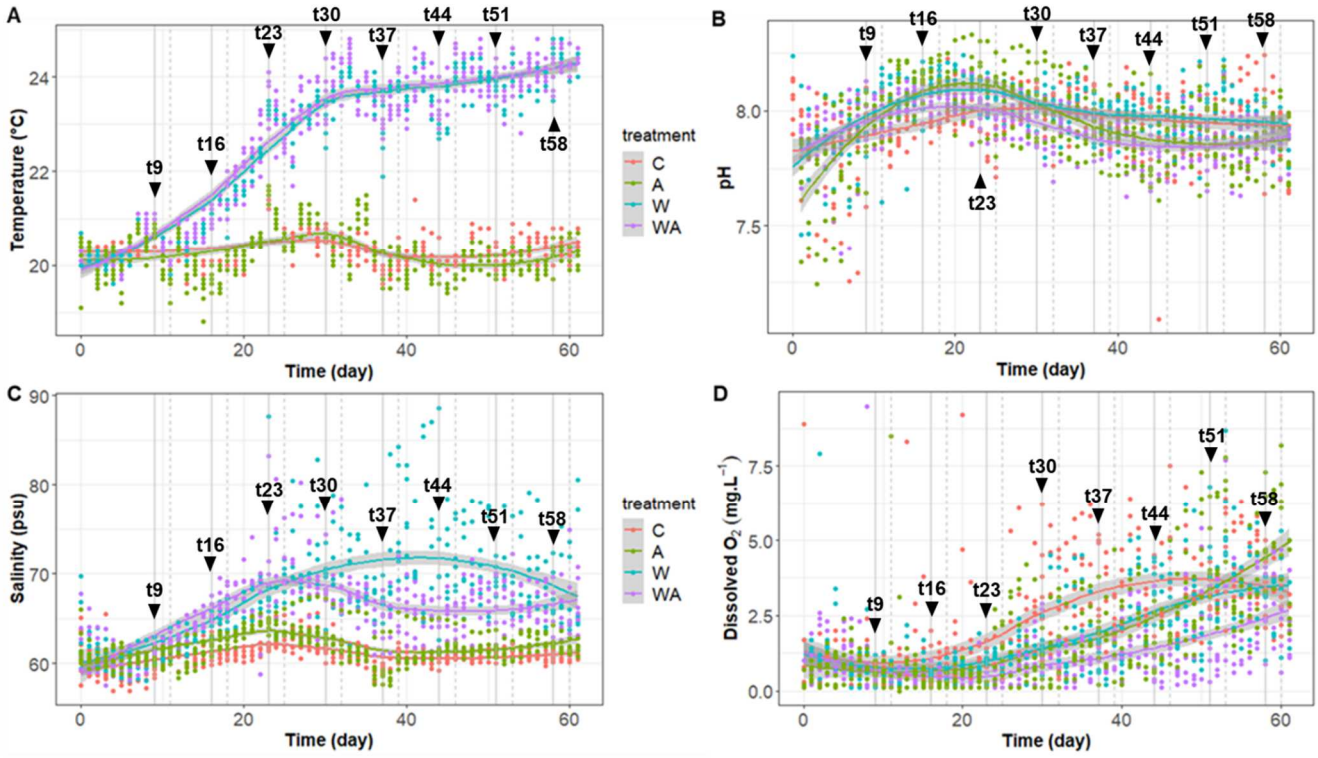

Figure 2: Temporal variation of the temperature (°C) **(A)**, the pH (upH) **(B)**, the salinity (psu) **(C)** and the dissolved oxygen (mg.L^{-1}) **(D)** of the different treatments (control (C), acidification (A), warming (W) or warming and acidification mix (WA)). The points corresponded to the values measured for each sample. The curves represented local regressions, based on the k-nearest neighbors algorithm (*geom_smooth* function of the ggplot2 package, loess method). The grey areas symbolised the 95% confidence intervals. The sampling days were represented by black arrows. The day 0 to day 8 corresponded to the stabilisation week.

3.2 Pigment composition

A total of 37 pigments were identified. The analysis revealed the presence of several chlorophyll: chlorophyll *a* (C*a*) and corresponding epimers and allomers, chlorophyll *b* (C*b*)

339 and chlorophyll *c2* (C*c2*). Bacteriochlorophyll *a* (BC*a*) was identified as well as echinenone,
340 oscillol diquinovoside, myxol quinovoside and zeaxanthin. Other pigments were identified
341 including lutein, alloxanthin, carotenoids and canthaxanthins and its isomers. Pigments
342 corresponding to alteration products were also found: pyropheophytin, pheophytin *a*,
343 pheophorbide *a* and chlorophyllide *a*. The presence of non-identified chlorophyll *a*-like
344 molecules was also observed and hereby called chlorophyll derivatives (C deriv. #1-6).

345 **Table 1:** Pigments identified by HPLC and its corresponding abbreviations.

Pigment	Notation
alpha and beta Cryptoxanthin	aCy; bCy
Alloxanthin	Al
Beta-beta caroten; beta-epsilon caroten	BB.Car; BE.Car
Unknown carotenoids	Car1; Car2
Chlorophyll *a* ; Chlorophyll *a* allomers/epimers	C*a*; C*a*.allo; C*a*.epi
Chlorophyll derivatives	C deriv. #1-6
Bacteriochlorophyll *a*	BC*a*
Chlorophyll *b*	Cb
Chlorophyll *c2*	Cc2
Chlorophyllide *a*	Cda
Canthaxanthin	Ct; Ct.iso
Echinenone	Ec
Fucoxanthin and isomers	F; F.iso1
Lutein and isomers	L; L.iso1; L.iso2
Myxol quinovoside and isomers	My.iso1; My.iso2; My.iso3; My.iso4
Oscillol diquinovoside	O
Pheophorbide	Pda.1
Pheophytin	Pha
Pyropheophytin	Pya
Zeaxanthin	Z

346

347 3.3 Acidification changes the pigments dynamics

348

349 At t9, all treatments were placed under the same water temperature and pH. No difference
350 between pigments were observed (Fig.3) (ANOVA or Welch or Kruskal, $p>0.05$).
351 The C treatment was different form the other treatments containing more myxol quinovoside
352 and isomers 2 and 3 than A treatment at t37 and t44 (Kruskal, $p<0.05$) and than the three
353 other treatments at t51 (ANOVA, $p<0.05$). It also contained more chlorophyll epimers at t58
354 than A, W and WA treatments (ANOVA, $p<0.05$) (Fig.3). The W treatment was differentiated
355 from the A treatment with the presence of chlorophyll derivative #6 at t51 and t58 (Welch,

356 p<0.05) (Fig.3). The concentration of chlorophyll *a* was around 4% at the beginning of the
357 experiment (Fig. 4, A). It increased until t51 in all treatments except for A treatment and then
358 decreased at t58 (Fig. 4, A). The A treatment slightly decreased at t58 and the proportion of
359 chlorophyll *a* was lower in this treatment than in the C treatment (ANOVA, $p < 0.05$) at t51
360 and t58 (Fig. 4, A). Conversely, the proportion of chlorophyll derivatives (Fig. 4, B) was close
361 to 0 at t9 for all treatments. It increased to t30, remained stable at t44 and then decreased
362 again to t58 for the C, W and WA groups, while it increased to t44 before decreasing again to
363 t58 for the A group (Fig. 4, B). The proportion of chlorophyll derivatives was significantly
364 higher for the A treatment at t37, t44 and t51 (ANOVA and Welch, $p < 0.05$) (Fig. 4, B).

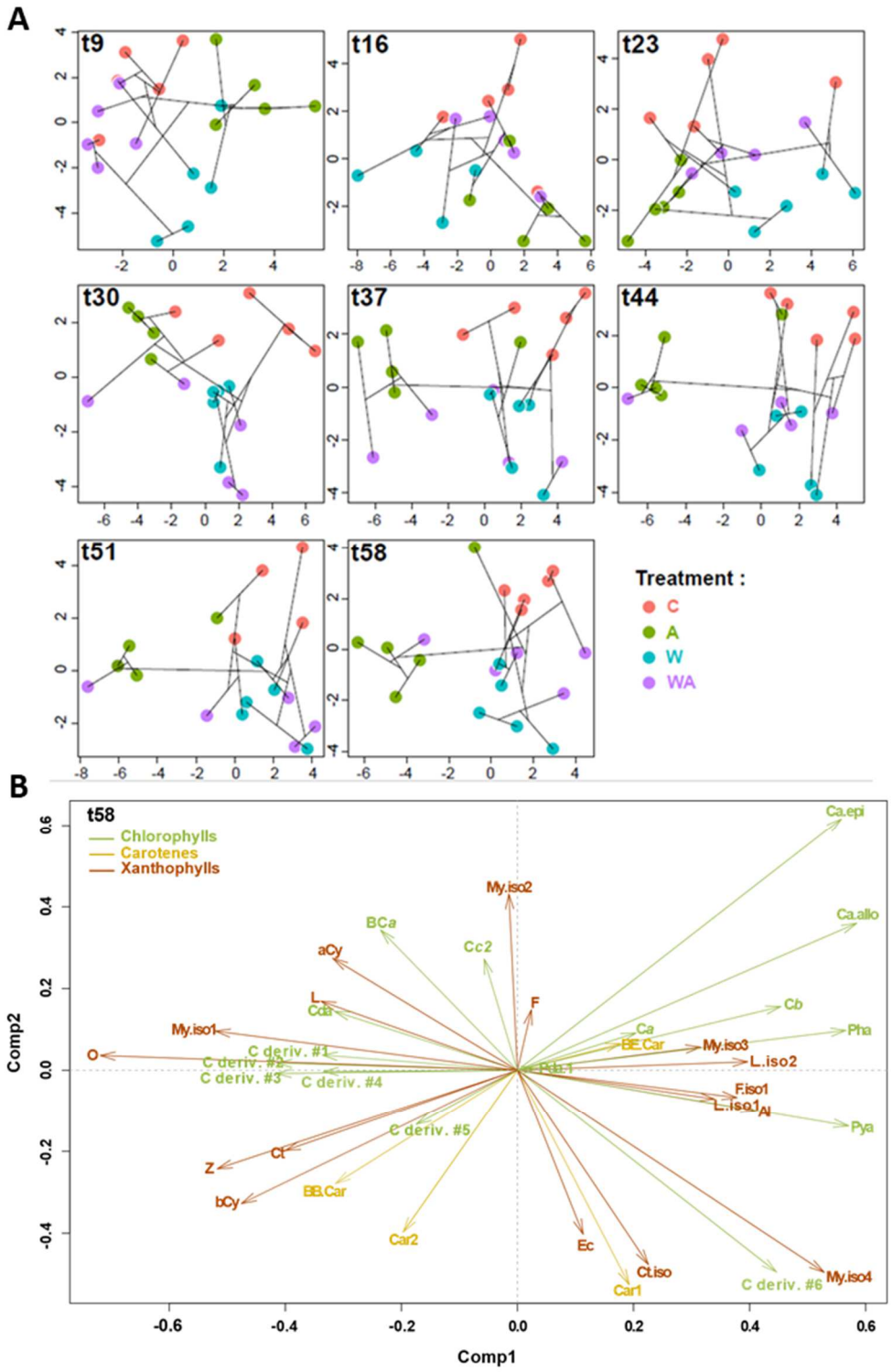

Figure 3: Dynamics of microbial communities according to pigments composition and the sampling time (tX) **(A)**. This figure was obtained thanks to analyze BCA combined with hierarchical cluster analysis with a Bray dissimilarity index and ward.D2 method. A representation more detailed with the different parameters was done at t58 **(B)**. The correspondence between the abbreviations and the names of pigments is provided on the **table 1**.

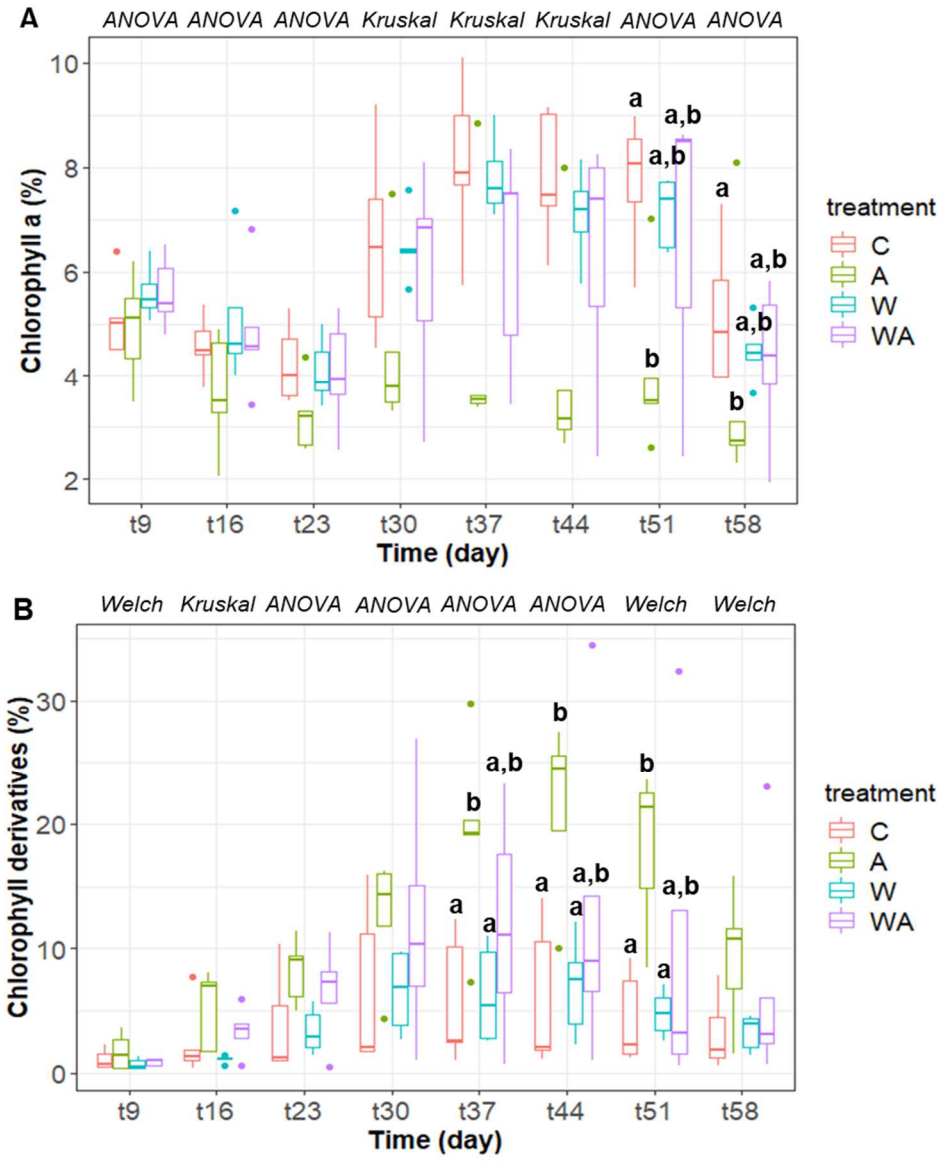

<u>Figure 4:</u> Temporal variations of **(A)** the concentration of chlorophyll *a* (%) and **(B)** the concentration of chlorophyll derivatives (%). The letters t followed by a number indicates the sampling time. The statistical test performed to show the differences between treatments at a sampling time is indicated in italics above the figure. The letters indicated a significant difference ($p < 0.05$) found after a post-hoc Tuckey test in the case of an ANOVA or a Games-Howell test in the case of a Welch ANOVA.

3.4 Comparison of the photosynthetic yields of the microbial mat in the different treatments

The quantum efficiency of photosystem II (ϕ(II)') indicated the photosynthetic efficiency of the mat. At t9, the quantum yields of the C and A treatments were close to 0, while those of the

W and WA groups were 14 and 4.2 times more than C and A treatments respectively (Fig. 5). At t16 no significant difference was observed between all the quantum yields (ANOVA, $p > 0.05$) (Fig. 5). Other difference were observed between treatments during the experiment, but the kinetics obtained showed no real trend between treatments (Fig. 5), only WA treatment presented a quantum yields lower than C treatment at t37, t51 and t58 (ANOVA or Kruskal, $p<0.05$) than W and A treatments at t37 and t58 (ANOVA, $p<0.05$).

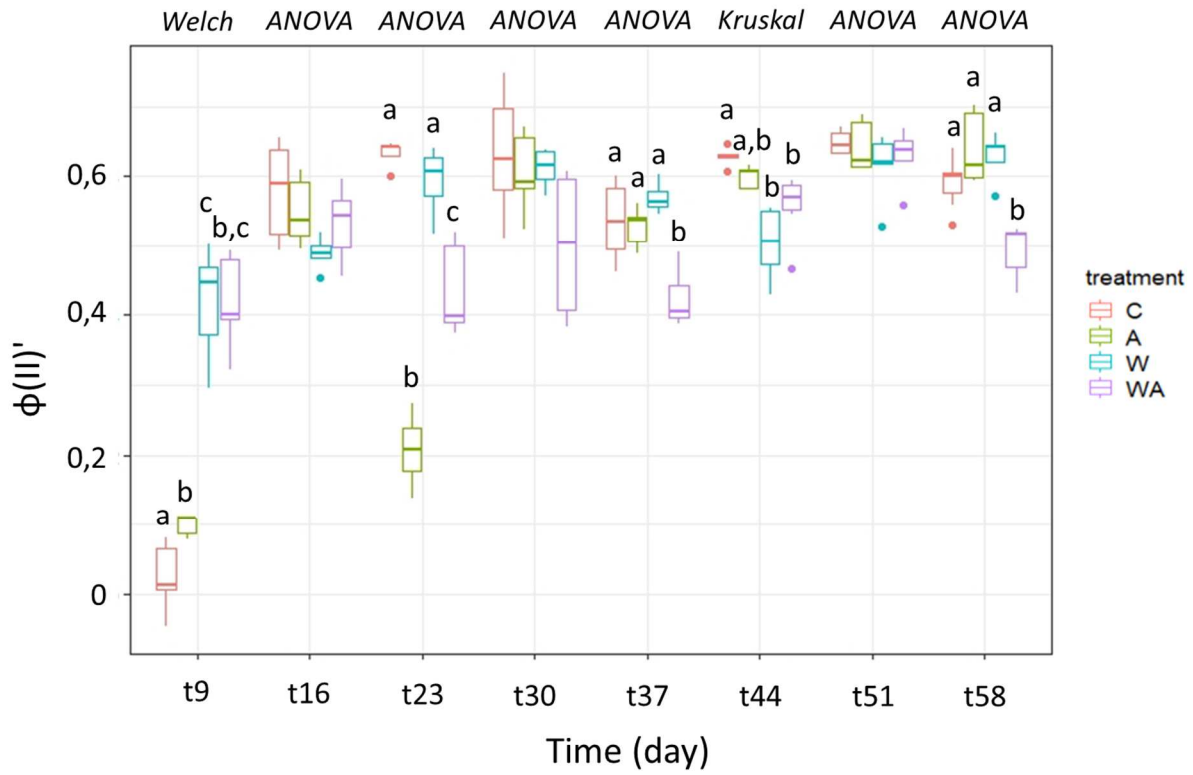

Figure 5: Variation of the quantum efficiency of photosystem II (ϕ(II)') in the different treatment. The letters t followed by a number indicates the sampling time. Above the figure was indicated in italics the test carried out for the comparison between treatments of the same week. The letters indicated a significant difference ($p < 0.05$) found after a post-hoc Tukey HSD test in the case of an ANOVA, a Games-Howell test in the case of a Welch ANOVA or a Nemenyi test in the case of a Kruskal Wallis test.

3.5 Acidification impacted the proportion of EPS

The A treatment was dissimilar from the other treatments, characterized by its higher concentrations of bound carbohydrates EPS.

The carbohydrates bound EPS concentration was notably more important in A treatment on three times: at t23, t37 and t58 (ANOVA, $p < 0.05$) (Fig. 6).

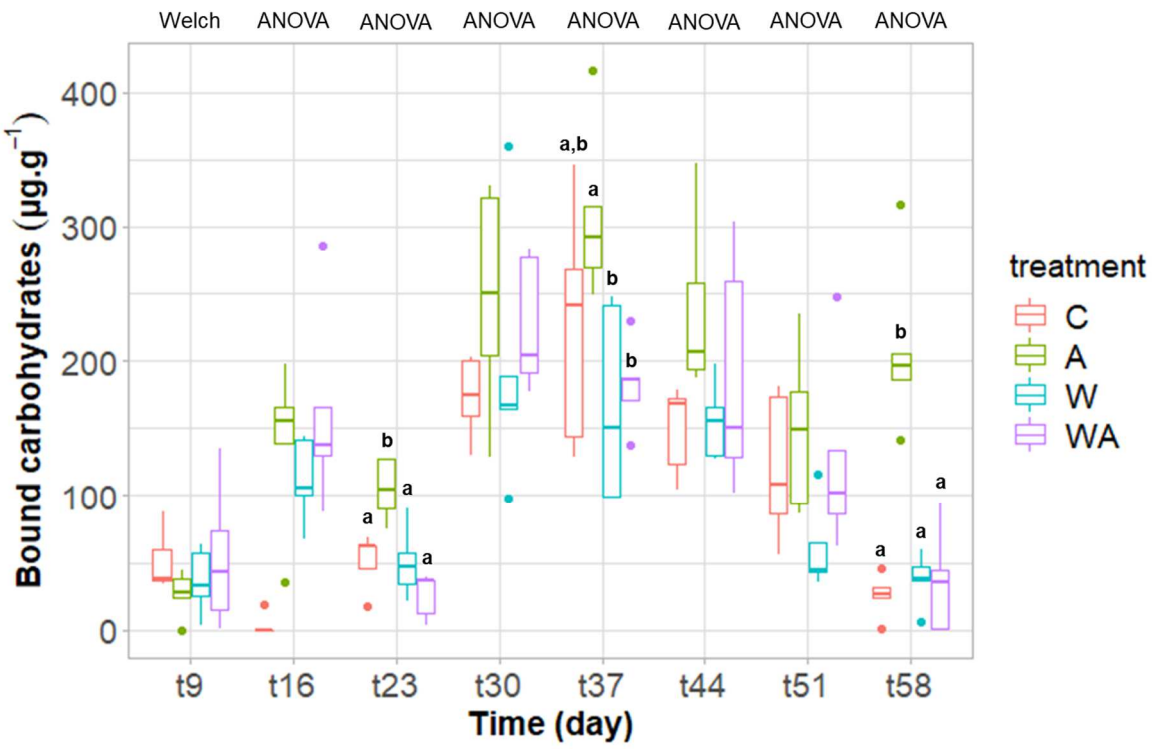

Figure 6: Temporal variation of the carbohydrate concentration in the bound fraction of EPS (in µg.g^{-1} dry mass). The letters t followed by a number indicates the sampling time. The statistical test performed to show the differences between treatments at a sampling time is indicated in italics above the figure. The letters indicate a significant difference ($p < 0.05$) found after a post-hoc Tuckey test. Note: the ANOVA performed at t16 did not consider the C treatment because of the presence of outliers.

4. Discussion

The aim of the study was to simulate acidification and/or warming on microbial mats. The mesocosm system has the advantage to control the physico-chemical parameters allowing to simulate future conditions, which is impossible to achieve directly in the field; but the natural environment can never be mimicked perfectly (weather, daily or even seasonal variations in physico-chemical parameters, *etc.*). Although mesocosm system will never faithfully represent reality, it is a compromise often used to conduct experimental ecology studies (Cravo-Laureau and Duran, 2014). It is therefore advisable to remain vigilant so as not to

423 extrapolate too generally the results obtained with *in situ* microbial mats. Given the diversity
424 of structure and functioning of microbial mats throughout the world, they may act differently in
425 their natural environment. It should also be noted that this study was a simulation of the
426 IPCC's most pessimistic predictions (RCP8.5) for 2100. The changes simulated only
427 concerned the decrease in water pH and the increase in water temperature, but these are
428 not the only parameters that are expected to vary in the future. Deoxygenation of the oceans,
429 a succession of extreme weather events, and sea level rise in some regions are also
430 foreseeable changes that have not been tested in this study. Moreover, they have been
431 monitored over seven weeks, whereas variations in the natural environment are supposed to
432 occur over several decades.

433 The renewal water in the mesocosm permitted to maintain a stable water level at 3 cm above
434 the mat and a natural supply of nutrients for the development of microbial mats. Redfield
435 ratio showed some limitation of nitrogen and/or phosphorus in the water under some
436 conditions but previous studies have shown that microbial mats can develop in P- (Peimbert
437 et al., 2012) and N-limited environment (Peimbert et al., 2012) (Supplementary materials, fig.
438 C).

439 Surprisingly, the decrease of pH under the A and WA treatments was not noticeable in the
440 mesocosms (Fig. 2) although the pH in the respective water reserve decreased
441 (Supplementary materials, fig. D) at the expected pH 7.6 (the initial pH was 8). This
442 phenomenon has been observed in other studies (Crawfurd et al., 2011; Ma et al., 2019).
443 The most likely hypothesis is that the rate of CO_2 fixation by photosynthesis was higher in the
444 A and WA treatments, which had the effect of increasing the pH. In our experiment, dissolved
445 oxygen increased under A treatment after the third week. Moreover, many microbial species
446 are able to use carbon concentration mechanisms (CCMs), storing high CO_2 concentrations
447 before transport into the Rubisco compartments, which minimise photorespiration. These
448 CCMs are found in oxygenic phototrophs like cyanobacteria or most of the phytoplankton
449 (Ma et al., 2019). The CCMs have been proposed as mechanisms to prevent photosynthetic

systems to directly detect ambient changes in CO_2 (Mackey et al., 2015). As a result, photosynthetic rates might not respond directly to ambient changes in CO_2 explaining the delay observed in the increase of dissolved oxygen in our experiment. Such observation is consistent with the fact that pH decreased from t23 while dissolved oxygen continued to increase (Fig. 2). Black et al. (2019) suggested that microphytobenthos use additional CO_2 due to acidification for photosynthesis until the maximum yield capacity has been reached. When the cells reached maximum intracellular CO_2 concentration through their CCMs, any additional CO_2 would contribute to the decrease in pH. The pH of the WA treatment followed the same dynamic as observed for the A treatment. However, the dissolved oxygen concentration under WA treatment increased less than half in comparison to the A treatment (Fig. 2, D). The CO_2 absorption mechanisms may have been less efficient in WA treatment because temperature decreases the solubility of CO_2 (Wootton et al., 2008).

Numerous studies have shown that photosystem II is very sensitive to environmental stress (Murata et al., 2007; Nishiyama et al., 2008; Wang et al., 2013). It is therefore important to focus on the quantum yield of photosystem II, which indicates the maximum photosynthetic activity potential of the communities. At t9, the quantum yield of photosystem II for the C and A treatments were close to 0 (Fig. 5), which indicated that the mats were not in good physiological condition when starting the experiment. Significantly lower quantum yields were observed under some treatments. At t23, under the A and the WA treatments an unexplained decrease of the quantum yield was observed (Fig. 5). The WA treatment exhibited significantly lower quantum yield than the other treatments at t37, t51 and t58 (Fig. 5), suggesting that mats have more difficulty withstanding simultaneous acidification and heating. It was not surprising that there was no difference in quantum efficiency between A and C treatments (Fig. 5). Photosynthetic organisms have a high capacity to modify pH with evidence that pH is regulated at the water/cell interface (Black et al., 2019). Our fluorometer illuminated with a blue LED emitter (455 nm). Chlorophyll *a* fluorescence per unit concentration in cyanobacteria tends to be lower than in algae when it is excited with blue

light. This leads to an erroneous biomass estimate of cyanobacteria. In their study, Simis *et al.* (2012) have sought the optimal excitation and emission pairs for the separation of cyanobacterial and algal Fv/Fm in communities. They demonstrate that the highest correlation between community and cyanobacterial variable fluorescence is obtained under orange-red excitation in the 590–650 nm range, exciting cyanobacterial phycobilipigments. No information was found about the other phototrophic communities.

The A treatment possessed more chlorophyll derivatives and lower chlorophyll *a* than the other treatments (Fig. 4). These chlorophyll derivatives molecules seemed to be bioindicators of a stress condition (water acidification). They were not identified by available standards. These molecules did not correspond to known metallised allomers or epimers of chlorophyll *a* (C*a*), as revealed by their retention time (Supplementary materials, fig. E). Based on their absorption spectra (Fig. 7), we can also rule out the hypothesis that these molecules correspond to de-metallised derivatives of chlorophyll *a* such as pheophytin *a* or pheophorbide *a* or even to bacteriochlorophyll *a* (BC*a*).

We can assume that these molecules correspond to transmetalated C*a* or BC*a*. Some microorganisms are known to possess bacteriochlorophyll those the central Mg ion is replaced by another metal, as observed for *Acidiphilium* where BC*a* possess a Zn central metal (Hiraishi and Shimada, 2001). This organism has been isolated from acidic mine ponds and it is supposed likely that pH constituted the evolutionary pressure responsible for the change of the central metal (Hiraishi and Shimada, 2001). Although this is an attractive hypothesis, it is highly unlikely that our pH treatment had the effect of promoting the synthesis of transmetalated BCa as Zn-BCa displays absorption features in the near infra-red range (Nagata et al., 2003) that were not observed here.

Chlorophylls and porphyrin derivatives generally have two major absorption bands (*i.e.* ‘‘red’’ (Q-) and ‘‘blue’’ (Soret-) bands, Fig. 7) in the visible range, due to extended π-delocalization at the edge of cyclic porphyrin skeleton (Milenković et al., 2012). Two main Q-bands ($Q_{y,0\text{-}0}$ and $Q_{y,0\text{-}1}$) are traditionally observed in the original C*a* (or Mg-C*a*) (Gerola et al., 2011). In our

504 case, C*a* wavelengths of maximum absorption λ_{max} were respectively 665 ($Q_{y,0-0}$) and 615 nm
505 ($Q_{y,0-1}$).

506 Based on these findings, the unidentified derivatives do not correspond to transmetalated
507 C*a*, although those absorption characteristics are close to the Mg-C*a* molecule. As shown
508 previously by Gerola *et al.* (2011), a hypsochromic (blue) shift of both Soret and $Q_{y,0-0}$ bands
509 must be expected with significant decreasing of λ_{max} in Zn- and Cu-C*a* in comparison to Mg-
510 C*a*. Such hypsochromic shifts were not observed in the unidentified derivatives spectra.

511 The only noticeable change corresponded to a decreased intensity (hypochromic effect) in
512 the $Q_{y,0-0}$ band in comparison with that of Mg-C*a* and a bathochromic (red) shift in the $Q_{y,0-1}$.
513 (Fig.7). These characteristics are similar to those of bacteriochlorophyll *c* (BC*c*) with a
514 recorded λ_{max} (630 nm) for $Q_{y,0-1}$ close to the expected 623-629 nm (Goedheer, 1966; Oelze,
515 1985; Pierson and Castenholz, 1974). This pigment is typically found in the chlorosomes of
516 green anoxygenic phototroph bacteria, including the green sulfur bacteria and the green non-
517 sulfur bacteria (Frigaard et al., 2006; Scheer, 2006), which indicated that the pH conditions
518 may have favoured the growth of these phototrophic bacteria.

519 Even moderate changes of both pH and temperature are relevant for bacterial community
520 composition of microbial mats (Uribe□Lorío et al., 2019). A decrease in chlorophyll *a* has
521 been observed under high CO_2 levels suggesting that the CO_2 input reduce CCMs and thus
522 save energy, particularly in pigment synthesis (Wang et al., 2019; Yue et al., 2019). In hot
523 springs from Costa Rica, significant changes of microbial mat communities were observed
524 with a significant increase of Chloroflexi (also named the green non-sulfur bacteria)
525 abundance with decreasing pH and increasing temperature (Uribe□Lorío et al., 2019).
526 Chloroflexi have been previously reported to be more abundant at decreased pH on
527 sediment of hydrothermal CO_2 seeps in Papua New Guinea (Hassenrück et al., 2016) and in
528 host-association with corals and sponges (Kandler et al., 2018; Morrow et al., 2015).
529 Chlorobi, the green sulfur bacteria, have also been found to increase in abundance with
530 acidification (Hassenrück et al., 2016). On their study, Hassenrück *et al*. (2016) supposed

that in the sites characterized by low pH and high hydrothermal influence, including pronounced temperature increases, the Chloroflexi and Chlorobi replaced other microbial communities as major carbon degraders under anoxic conditions. Green anoxygenic bacteria participate on the carbon cycling and have been shown to fix CO_2 (Hug et al., 2013; Sirevåg, 2004). The phototrophic communities of the microbial mats could be modified under A treatment leading to a higher relative abundance of green anoxygenic bacteria. It is also possible that the presence of more CO_2 on the environment conducted to a shift on the metabolism of green anoxygenic phototrophic bacteria fixing the CO_2 and being more competitive with the other communities.

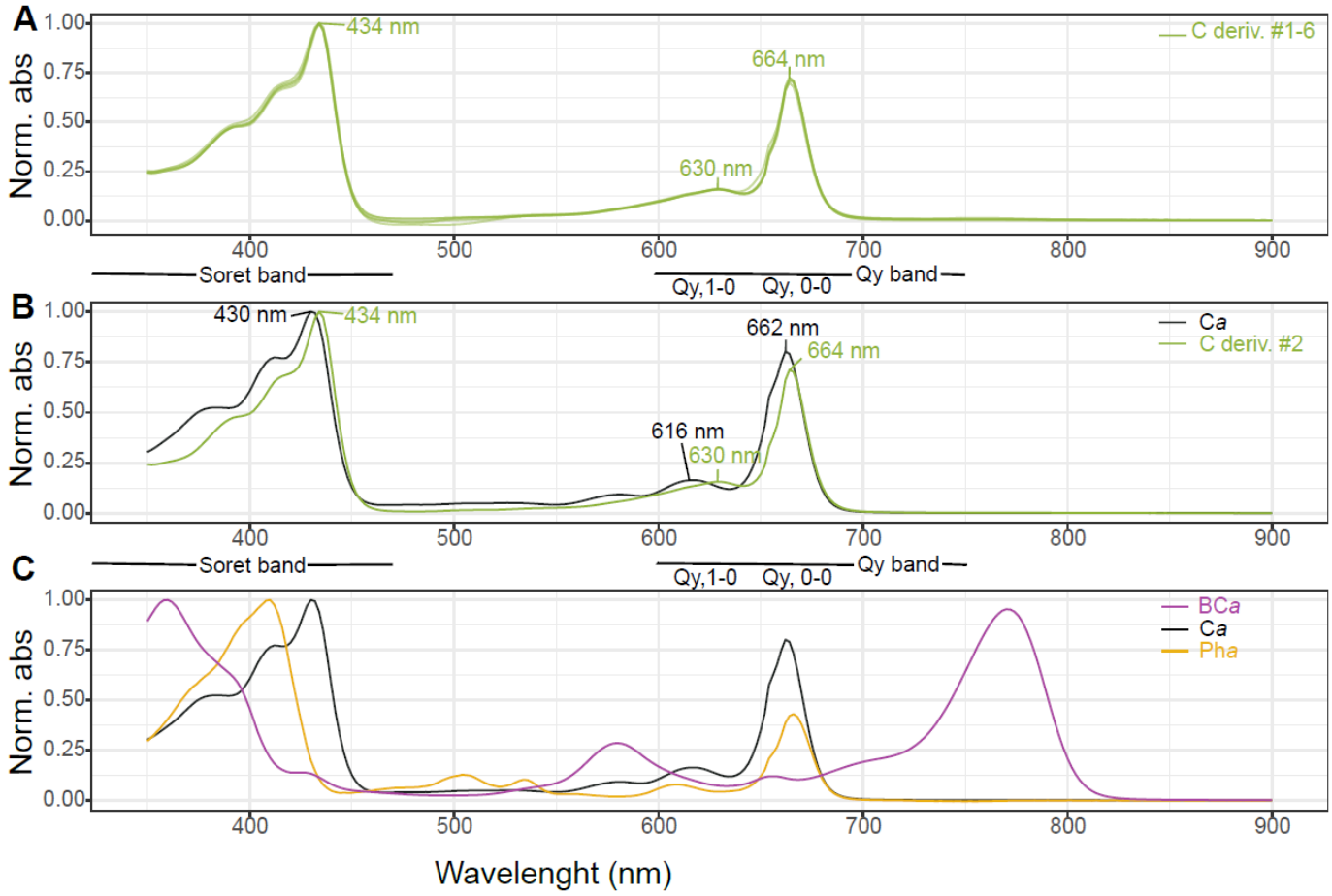

Figure 7: Normalized absorption spectra of different pigments of the microbial mats. **A**: superimposed absorption spectra of the 6 detected chlorophyll derivatives (C deriv.). **B**: comparison between the absorption spectra of chlorophyll *a* (C*a*) and C deriv. #2. **C**:

545 comparison between the absorption spectra of C*a*, pheophytin *a* (Ph*a*) and
546 bacteriochlorophyll *a* (BC*a*).
547
548 The bound carbohydrate EPS production was higher under the A treatment. EPS are
549 essential for maintaining the physical properties and proper functioning of microbial mats,
550 and are also involved in the adaptation of communities to their environment (Dupraz and
551 Visscher, 2005; Hubas, 2018; Prieto-Barajas et al., 2018). Therefore, EPS are an essential
552 element, even more when microorganisms are confronted with strong variations in physico-
553 chemical parameters. It has been observed that the degradation of polysaccharides by
554 bacterial extracellular enzymes is accelerated at low pH (Piontek et al., 2009). It can be
555 supposed that microbial mats could therefore synthesize more carbohydrates to compensate
556 for this degradation. Microbial mats in the W treatment did not show any variation in
557 concentration, suggesting that temperature has no effect on this process. Those in the WA
558 treatment also did not change suggesting that acidification and warming have probably
559 antagonistic effects limiting the impact of acidification on EPS. However, Li *et al.* (2016)
560 obtained contradictory results on three freshwater microalgae as they demonstrated that
561 acidification and warming act synergistically. The variation of bound carbohydrate EPS
562 suggest that microbial mats subjected to acidification modified their metabolism. Tan *et al.*
563 (2019) have shown that a polar strain of *Chlorella sp.* modulates its metabolism under
564 acidified conditions (pCO_2 = 1000 µatm), favouring its survival. They observed a decrease in
565 the fluxes of glucose and sucrose, the main products of photosynthesis, under high pCO_2.
566 Gong *et al.* (2020) also observed that the starch metabolism was modified by increasing the
567 quantity of starch granules in another microalgae named *Symbiochlorum hainanensis*. These
568 observations suggest that the organic carbon produced by photosynthesis in the microbial
569 mats placed under the A treatment was redirected towards the synthesis of other
570 carbohydrates which concentration had considerably increased.
571

572 ## 5. Conclusion

573 The temperature in the warming treatments increased by 4°C from the initial temperature as
574 expected. Despite of a decrease of 0.4 unit pH in the water reserves of acidification
575 treatments, no significance difference was observed between the water pH of the different
576 treatments. The salinity increased on the warming treatments because of the water
577 evaporation. The dissolved oxygen concentration increased and was higher on the
578 acidification treatments, certainly due to an increase of the photosynthesis because of the
579 carbon input.

580 In the acidification treatment, our results showed that the concentration of bound
581 carbohydrates EPS increased. This indicated that the metabolisms were modified to cope
582 with the induced changes. In addition, the phototrophic communities of the microbial mats
583 under the different treatments showed characteristic pigments. In particular, unknown
584 chlorophyll derivatives were present under acidification and/or warming treatments. To the
585 best of our knowledge the synthesis of such derivatives following an acidification or/and a
586 warming experiment has never been reported before. These molecules were eventually
587 identified as bacteriochlorophyll *c* and several possible isomers which suggest that
588 experimentally induced climate change scenario may have favoured the increase of BC*c*
589 contained on green anoxygenic phototroph bacteria.

590 The mesocosm experiment has shown that phototrophic communities of the microbial mats
591 were able to adapt to the conditions defined by the IPCC (2014) regarding acidification and
592 warming of surface water. The most probable explanation is that the studied microbial mats
593 are already naturally confronted with environmental conditions (pH, light, temperature,
594 salinity, *etc.*) that fluctuate with a great amplitude in salt marshes. They may therefore
595 already be confronted with temperature and pH conditions predicted, for example, by the
596 IPCC for 2100. Changes in their metabolism probably enabled them to maintain a high
597 potential for photosynthetic activity when acidification took place. In the future, it would be
598 interesting to observe if a difference in the phylogenetic composition of these communities
599 occurred. This study provides new insights on the response of phototrophic communities of

microbial mats in a context of climatic change and permit to better understand their function in this ecosystem.

Acknowledgements

C. Mazière was supported by a PhD grant from E2S-UPPA program and the Région Nouvelle-Aquitaine. We thank the funding support from the European programme ERANETMED AQUASALT (NMED-0003-01) and from the ACI politique d'établissement Université de La Rochelle.

The authors are grateful to the salterns owner Michel Jauffrais and Thomas Lacoue-Labarthe for his help in setting up the acidification treatment.

References

Aminot, A., Kérouel, R., 2007. Dosage automatique des nutriments dans les eaux marines., Quae. ed.

Baragi, L.V., Anil, A.C., 2016. Synergistic effect of elevated temperature, pCO 2 and nutrients on marine biofilm. Mar. Pollut. Bull. 105, 102–109. https://doi.org/10.1016/j.marpolbul.2016.02.049

Baragi, L.V., Khandeparker, L., Anil, A.C., 2015. Influence of elevated temperature and pCO2 on the marine periphytic diatom Navicula distans and its associated organisms in culture. Hydrobiologia 762, 127–142. https://doi.org/10.1007/s10750-015-2343-9

Beardall, J., Stojkovic, S., Larsen, S., 2009. Living in a high CO2 world: Impacts of global climate change on marine phytoplankton. Plant Ecol. Divers. 2, 191–205. https://doi.org/10.1080/17550870903271363

Black, J.G., Stark, J.S., Johnstone, G.J., McMinn, A., Boyd, P., McKinlay, J., Wootherspoon, S., Runcie, J.W., 2019. In-situ behavioural and physiological responses of Antarctic microphytobenthos to ocean acidification. Sci. Rep. 9, 1890. https://doi.org/10.1038/s41598-018-36233-2

Bolhuis, H., Stal, L.J., 2011. Analysis of bacterial and archaeal diversity in coastal microbial mats using massive parallel 16S rRNA gene tag sequencing. ISME J. 5, 1701–1712. https://doi.org/10.1038/ismej.2011.52

Bordenave, S., Fourçans, A., Blanchard, S., Goñi, M.S., Caumette, P., Duran, R., 2004a. Structure and functional analyses of bacterial communities changes in microbial mats following petroleum exposure. Ophelia 58, 195–203. https://doi.org/10.1080/00785236.2004.10410227

Bordenave, S., Goñi-urriza, M., Vilette, C., Blanchard, S., Caumette, P., Duran, R., 2008. Diversity of ring-hydroxylating dioxygenases in pristine and oil contaminated microbial mats at genomic and transcriptomic levels. Environ. Microbiol. 10, 3201–3211. https://doi.org/10.1111/j.1462-2920.2008.01707.x

Bordenave, S., Jézéquel, R., Fourçans, A., Budzinski, H., Merlin, F.X., Fourel, T., Goñi-Urriza, M., Guyoneaud, R., Grimaud, R., Caumette, P., Duran, R., 2004b. Degradation of the "Erika" oil. Aquat. Living Resour. 17, 261–267. https://doi.org/10.1051/alr:2004027

639 Brotas, V., Plante-Cuny, M.-R., 2003. The use of HPLC pigment analysis to study microphytobenthos
640 communities. Acta Oecologica 24. https://doi.org/10.1016/S1146-609X(03)00013-4
641 Cartaxana, P., Vieira, S., Ribeiro, L., Rocha, R., Cruz, S., Calado, R., Marques da Silva, J., 2015. Effects
642 of elevated temperature and CO2 on intertidal microphytobenthos. BMC Ecol. 15, 10.
643 https://doi.org/10.1186/s12898-015-0043-y
644 Cavicchioli, R., Ripple, W.J., Timmis, K.N., Azam, F., Bakken, L.R., Baylis, M., Behrenfeld, M.J., Boetius,
645 A., Boyd, P.W., Classen, A.T., Crowther, T.W., Danovaro, R., Foreman, C.M., Huisman, J.,
646 Hutchins, D.A., Jansson, J.K., Karl, D.M., Koskella, B., Mark Welch, D.B., Martiny, J.B.H.,
647 Moran, M.A., Orphan, V.J., Reay, D.S., Remais, J.V., Rich, V.I., Singh, B.K., Stein, L.Y., Stewart,
648 F.J., Sullivan, M.B., van Oppen, M.J.H., Weaver, S.C., Webb, E.A., Webster, N.S., 2019.
649 Scientists' warning to humanity: microorganisms and climate change. Nat. Rev. Microbiol. 17,
650 569–586. https://doi.org/10.1038/s41579-019-0222-5
651 Cravo-Laureau, C., Duran, R., 2014. Marine coastal sediments microbial hydrocarbon degradation
652 processes: contribution of experimental ecology in the omics'era. Front. Microbiol. 5.
653 https://doi.org/10.3389/fmicb.2014.00039
654 Crawfurd, K.J., Raven, J.A., Wheeler, G.L., Baxter, E.J., Joint, I., 2011. The Response of Thalassiosira
655 pseudonana to Long-Term Exposure to Increased CO2 and Decreased pH. PLoS ONE 6,
656 e26695. https://doi.org/10.1371/journal.pone.0026695
657 Decho, A., 2000. Microbial biofilms in intertidal systems: an overview. Cont. Shelf Res. 20, 1257–
658 1273. https://doi.org/10.1016/S0278-4343(00)00022-4
659 Decho, A., 1990. Decho AW.. Microbial exopolymer secretions in ocean environments: their role(s) in
660 food webs and marine processes. Oceanogr Mar Biol Ann Rev 28: 73-153. Oceanogr. Mar.
661 Biol. Annu. Rev. 28, 73–154.
662 Decho, A.W., Moriarty, D.J.W., 1990. Bacterial exopolymer utilization by a harpacticoid copepod: A
663 methodology and results. Limnol. Oceanogr. 35, 1039–1049.
664 https://doi.org/10.4319/lo.1990.35.5.1039
665 Dobretsov, S., Abed, R.M.M., Al Maskari, S.M.S., Al Sabahi, J.N., Victor, R., 2011. Cyanobacterial mats
666 from hot springs produce antimicrobial compounds and quorum-sensing inhibitors under
667 natural conditions. J. Appl. Phycol. 23, 983–993. https://doi.org/10.1007/s10811-010-9627-2
668 Dubois, Michel., Gilles, K.A., Hamilton, J.K., Rebers, P.A., Smith, Fred., 1956. Colorimetric Method for
669 Determination of Sugars and Related Substances. Anal. Chem. 28, 350–356.
670 https://doi.org/10.1021/ac60111a017
671 Dupraz, C., Visscher, P.T., 2005. Microbial lithification in marine stromatolites and hypersaline mats.
672 Trends Microbiol. 13, 429–438. https://doi.org/10.1016/j.tim.2005.07.008
673 Dutta, H., Dutta, A., 2016. The microbial aspect of climate change. Energy Ecol. Environ. 1, 209–232.
674 https://doi.org/10.1007/s40974-016-0034-7
675 Flemming, H.-C., Wingender, J., 2010. The biofilm matrix. Nat. Rev. Microbiol. 8, 623–633.
676 https://doi.org/10.1038/nrmicro2415
677 Fourçans, A., Oteyza, T.G. de, Wieland, A., Solé, A., Diestra, E., Bleijswijk, J. van, Grimalt, J.O., Kühl,
678 M., Esteve, I., Muyzer, G., Caumette, P., Duran, R., 2004. Characterization of functional
679 bacterial groups in a hypersaline microbial mat community (Salins-de-Giraud, Camargue,
680 France). FEMS Microbiol. Ecol. 51, 55–70. https://doi.org/10.1016/j.femsec.2004.07.012
681 Fourçans, A., Ranchou-Peyruse, A., Caumette, P., Duran, R., 2008. Molecular Analysis of the Spatio-
682 temporal Distribution of Sulfate-reducing Bacteria (SRB) in Camargue (France) Hypersaline
683 Microbial Mat. Microb. Ecol. 56, 90–100. https://doi.org/10.1007/s00248-007-9327-x
684 Fourçans, A., Solé, A., Diestra, E., Ranchou-Peyruse, A., Esteve, I., Caumette, P., Duran, R., 2006.
685 Vertical migration of phototrophic bacterial populations in a hypersaline microbial mat from
686 Salins-de-Giraud (Camargue, France). FEMS Microbiol. Ecol. 57, 367–377.
687 https://doi.org/10.1111/j.1574-6941.2006.00124.x
688 Frigaard, N.-U., Maqueo Chew, A.G., Maresca, J.A., Bryant, D.A., 2006. Bacteriochlorophyll
689 Biosynthesis in Green Bacteria, in: Grimm, B., Porra, R.J., Rüdiger, W., Scheer, H. (Eds.),

690 Chlorophylls and Bacteriochlorophylls, Advances in Photosynthesis and Respiration. Springer
691 Netherlands, Dordrecht, pp. 201–221. https://doi.org/10.1007/1-4020-4516-6_15
692 Gao, K., Helbling, E., Häder, D., Hutchins, D., 2012. Responses of marine primary producers to
693 interactions between ocean acidification, solar radiation, and warming. Mar. Ecol. Prog. Ser.
694 470, 167. https://doi.org/10.3354/meps10043
695 Gerola, A.P., Tsubone, T.M., Santana, A., de Oliveira, H.P.M., Hioka, N., Caetano, W., 2011. Properties
696 of Chlorophyll and Derivatives in Homogeneous and Microheterogeneous Systems. J. Phys.
697 Chem. B 115, 7364–7373. https://doi.org/10.1021/jp201278b
698 Gette-Bouvarot, M., Mermillod-Blondin, F., Lemoine, D., Delolme, C., Danjean, M., Etienne, L.,
699 Volatier, L., 2015. The potential control of benthic biofilm growth by macrophytes—A
700 mesocosm approach. Ecol. Eng. 75, 178–186. https://doi.org/10.1016/j.ecoleng.2014.12.001
701 Goedheer, J.C., 1966. Visible Absorption and Fluorescence of Chlorophyll and Its Aggregates in
702 Solution, in: The Chlorophylls. Elsevier, pp. 147–184. https://doi.org/10.1016/B978-1-4832-
703 3289-8.50012-6
704 Gong, S., Jin, X., Xiao, Y., Li, Z., 2020. Ocean Acidification and Warming Lead to Increased Growth and
705 Altered Chloroplast Morphology in the Thermo-Tolerant Alga Symbiochlorum hainanensis.
706 Front. Plant Sci. 11. https://doi.org/10.3389/fpls.2020.585202
707 Hancke, K., Glud, R., 2004. Temperature effects on respiration and photosynthesis in three diatom-
708 dominated benthic communities. Aquat. Microb. Ecol. 37, 265–281.
709 https://doi.org/10.3354/ame037265
710 Hassenrück, C., Fink, A., Lichtschlag, A., Tegetmeyer, H.E., de Beer, D., Ramette, A., 2016.
711 Quantification of the effects of ocean acidification on sediment microbial communities in the
712 environment: the importance of ecosystem approaches. FEMS Microbiol. Ecol. 92.
713 https://doi.org/10.1093/femsec/fiw027
714 Hicks, N., Bulling, M.T., Solan, M., Raffaelli, D., White, P.C., Paterson, D.M., 2011. Impact of
715 biodiversity-climate futures on primary production and metabolism in a model benthic
716 estuarine system. BMC Ecol. 11, 7. https://doi.org/10.1186/1472-6785-11-7
717 Hiraishi, A., Shimada, K., 2001. Aerobic anoxygenic photosynthetic bacteria with zinc-
718 bacteriochlorophyll. J. Gen. Appl. Microbiol. 47, 161–180.
719 https://doi.org/10.2323/jgam.47.161
720 Hubas, C., 2018. Biofilms, tapis et agrégats microbiens : vers une vision unificatrice (HDR (Habilitation
721 à Diriger les Recherches)). Muséum National D'Histoire Naturelle.
722 https://doi.org/10.5281/zenodo.3784703
723 Hug, L.A., Castelle, C.J., Wrighton, K.C., Thomas, B.C., Sharon, I., Frischkorn, K.R., Williams, K.H.,
724 Tringe, S.G., Banfield, J.F., 2013. Community genomic analyses constrain the distribution of
725 metabolic traits across the Chloroflexi phylum and indicate roles in sediment carbon cycling.
726 Microbiome 1, 22. https://doi.org/10.1186/2049-2618-1-22
727 Hutchins, D.A., Fu, F., 2017. Microorganisms and ocean global change. Nat. Microbiol. 2, 17058.
728 https://doi.org/10.1038/nmicrobiol.2017.58
729 IPCC, 2014. Climate Change 2014: Synthesis Report. Contribution of Working Groups I, II and III
730 to the Fifth Assessment Report of the Intergovernmental Panel on Climate Change 169.
731 Jesus, B., Perkins, R.G., Mendes, C.R., Brotas, V., Paterson, D.M., 2006. Chlorophyll fluorescence as a
732 proxy for microphytobenthic biomass: alternatives to the current methodology. Mar. Biol.
733 150, 17–28. https://doi.org/10.1007/s00227-006-0324-2
734 Jorgensen, B.B., Revsbech, N.P., Cohen, Y., 1983. Photosynthesis and structure of benthic microbial
735 mats: Microelectrode and SEM studies of four cyanobacterial communities1. Limnol.
736 Oceanogr. 28, 1075–1093. https://doi.org/10.4319/lo.1983.28.6.1075
737 Kandler, N.M., Abdul Wahab, M.A., Noonan, S.H.C., Bell, J.J., Davy, S.K., Webster, N.S., Luter, H.M.,
738 2018. In situ responses of the sponge microbiome to ocean acidification. FEMS Microbiol.
739 Ecol. 94. https://doi.org/10.1093/femsec/fiy205

Li, W., Xu, X., Fujibayashi, M., Niu, Q., Tanaka, N., Nishimura, O., 2016. Response of microalgae to elevated CO2 and temperature: impact of climate change on freshwater ecosystems. Environ. Sci. Pollut. Res. 23, 19847–19860. https://doi.org/10.1007/s11356-016-7180-5

Ma, J., Wang, P., Wang, X., Xu, Y., Paerl, H.W., 2019. Cyanobacteria in eutrophic waters benefit from rising atmospheric CO2 concentrations. Sci. Total Environ. 691, 1144–1154. https://doi.org/10.1016/j.scitotenv.2019.07.056

Mackey, K., Morris, J., Morel, F., Kranz, S., 2015. Response of Photosynthesis to Ocean Acidification. Oceanography 25, 74–91. https://doi.org/10.5670/oceanog.2015.33

Milenković, S.M., Zvezdanović, J.B., Anđelković, T.D., Marković, D.Z., 2012. THE IDENTIFICATION OF CHLOROPHYLL AND ITS DERIVATIVES IN THE PIGMENT MIXTURES: HPLC-CHROMATOGRAPHY, VISIBLE AND MASS SPECTROSCOPY STUDIES. Adv. Technol. 9.

Morrow, K.M., Bourne, D.G., Humphrey, C., Botté, E.S., Laffy, P., Zaneveld, J., Uthicke, S., Fabricius, K.E., Webster, N.S., 2015. Natural volcanic CO 2 seeps reveal future trajectories for host–microbial associations in corals and sponges. ISME J. 9, 894–908. https://doi.org/10.1038/ismej.2014.188

Murata, N., Takahashi, S., Nishiyama, Y., Allakhverdiev, S.I., 2007. Photoinhibition of photosystem II under environmental stress. Biochim. Biophys. Acta BBA - Bioenerg., Structure and Function of Photosystems 1767, 414–421. https://doi.org/10.1016/j.bbabio.2006.11.019

Nagata, M., Yoshimura, Y., Inagaki, J., Suemori, Y., Iida, K., Ohtsuka, T., Nango, M., 2003. Construction and Photocurrent of Light-harvesting Polypeptides/Zinc Bacteriochlorophyll *a* Complex in Lipid Bilayers. Chem. Lett. 32, 852–853. https://doi.org/10.1246/cl.2003.852

Nishiyama, Y., Allakhverdiev, S.I., Murata, N., 2008. Regulation by Environmental Conditions of the Repair of Photosystem II in Cyanobacteria, in: Demmig-Adams, B., Adams, W.W., Mattoo, A.K. (Eds.), Photoprotection, Photoinhibition, Gene Regulation, and Environment, Advances in Photosynthesis and Respiration. Springer Netherlands, Dordrecht, pp. 193–203. https://doi.org/10.1007/1-4020-3579-9_13

Oelze, J., 1985. 9 Analysis of Bacteriochlorophylls**Dedicated to Prof. Dr. N. Pfennig on the occasion of his 60th birthday in recognition of his numerous contributions on the ecology and taxonomy of phototrophic bacteria., in: Bergan, T. (Ed.), Methods in Microbiology. Academic Press, pp. 257–284. https://doi.org/10.1016/S0580-9517(08)70478-1

Peimbert, M., Alcaraz, L.D., Bonilla-Rosso, G., Olmedo-Alvarez, G., García-Oliva, F., Segovia, L., Eguiarte, L.E., Souza, V., 2012. Comparative Metagenomics of Two Microbial Mats at Cuatro Ciénegas Basin I: Ancient Lessons on How to Cope with an Environment Under Severe Nutrient Stress. Astrobiology 12, 648–658. https://doi.org/10.1089/ast.2011.0694

Pierson, B.K., Castenholz, R.W., 1974. A phototrophic gliding filamentous bacterium of hot springs, Chloroflexus aurantiacus, gen. and sp. nov. Arch. Microbiol. 100, 5–24. https://doi.org/10.1007/BF00446302

Piontek, J., Lunau, M., Händel, N., Borchard, C., Wurst, M., Engel, A., 2009. Acidification increases microbial polysaccharide degradation in the ocean. Biogeosciences Discuss. 7. https://doi.org/10.5194/bg-7-1615-2010

Prieto-Barajas, C.M., Valencia-Cantero, E., Santoyo, G., 2018. Microbial mat ecosystems: Structure types, functional diversity, and biotechnological application. Electron. J. Biotechnol. 31, 48–56. https://doi.org/10.1016/j.ejbt.2017.11.001

Rae, B.D., Long, B.M., Badger, M.R., Price, G.D., 2013. Functions, Compositions, and Evolution of the Two Types of Carboxysomes: Polyhedral Microcompartments That Facilitate CO2 Fixation in Cyanobacteria and Some Proteobacteria. Microbiol. Mol. Biol. Rev. MMBR 77, 357–379. https://doi.org/10.1128/MMBR.00061-12

Redfield, A.C., 1958. The biological control of chemical factors in the environment. Am. Sci. 46, 230A–221.

Reinold, Wong, MacLeod, Meltzer, Thompson, Burns, 2019. The Vulnerability of Microbial Ecosystems in A Changing Climate: Potential Impact in Shark Bay. Life 9, 71. https://doi.org/10.3390/life9030071

792 Revsbech, N.P., Jorgensen, B.B., Blackburn, T.H., Cohen, Y., 1983. Microelectrode studies of the
793 photosynthesis and O2, H2S, and pH profiles of a microbial mat1. Limnol. Oceanogr. 28,
794 1062–1074. https://doi.org/10.4319/lo.1983.28.6.1062
795 Scheer, H., 2006. An Overview of Chlorophylls and Bacteriochlorophylls: Biochemistry, Biophysics,
796 Functions and Applications, in: Grimm, B., Porra, R.J., Rüdiger, W., Scheer, H. (Eds.),
797 Chlorophylls and Bacteriochlorophylls: Biochemistry, Biophysics, Functions and Applications,
798 Advances in Photosynthesis and Respiration. Springer Netherlands, Dordrecht, pp. 1–26.
799 https://doi.org/10.1007/1-4020-4516-6_1
800 Sirevåg, R., 2004. Carbon Metabolism in Green Bacteria, in: Blankenship, R.E., Madigan, M.T., Bauer,
801 C.E. (Eds.), Anoxygenic Photosynthetic Bacteria, Advances in Photosynthesis and Respiration.
802 Kluwer Academic Publishers, Dordrecht, pp. 871–883. https://doi.org/10.1007/0-306-47954-
803 0_40
804 Sørensen, K.B., Canfield, D.E., Teske, A.P., Oren, A., 2005. Community Composition of a Hypersaline
805 Endoevaporitic Microbial Mat. Appl. Environ. Microbiol. 71, 7352–7365.
806 https://doi.org/10.1128/AEM.71.11.7352-7365.2005
807 Stauffert, M., Cravo-Laureau, C., Jezequel, R., Barantal, S., Cuny, P., Gilbert, F., Cagnon, C., Militon, C.,
808 Amouroux, D., Mahdaoui, F., Bouyssiere, B., Stora, G., Merlin, F., Duran, R., 2013. Impact of
809 Oil on Bacterial Community Structure in Bioturbated Sediments. PloS One 8, e65347.
810 https://doi.org/10.1371/journal.pone.0065347
811 Takahashi, E., Ledauphin, J., Goux, D., Orvain, F., 2009. Optimising extraction of extracellular
812 polymeric substances (EPS) from benthic diatoms: Comparison of the efficiency of six EPS
813 extraction methods. Mar. Freshw. Res. 60, 1201–1210. http://dx.doi.org/10.1071/MF08258
814 Tan, Y.-H., Lim, P.-E., Beardall, J., Poong, S.-W., Phang, S.-M., 2019. A metabolomic approach to
815 investigate effects of ocean acidification on a polar microalga Chlorella sp. Aquat. Toxicol.
816 217, 105349. https://doi.org/10.1016/j.aquatox.2019.105349
817 Underwood, G.J.C., Boulcott, M., Raines, C.A., Waldron, K., 2004. Environmental Effects on
818 Exopolymer Production by Marine Benthic Diatoms: Dynamics, Changes in Composition, and
819 Pathways of Production1. J. Phycol. 40, 293–304. https://doi.org/10.1111/j.1529-
820 8817.2004.03076.x
821 Uribe-Lorío, L., Brenes-Guillén, L., Hernández-Ascencio, W., Mora-Amador, R., González, G., Ramírez-
822 Umaña, C.J., Díez, B., Pedrós-Alió, C., 2019. The influence of temperature and pH on bacterial
823 community composition of microbial mats in hot springs from Costa Rica. MicrobiologyOpen
824 8. https://doi.org/10.1002/mbo3.893
825 van Gemerden, H., 1993. Microbial mats: A joint venture. Mar. Geol. 113, 3–25.
826 https://doi.org/10.1016/0025-3227(93)90146-M
827 Wang, S., Zhang, D., Pan, X., 2013. Effects of cadmium on the activities of photosystems of Chlorella
828 pyrenoidosa and the protective role of cyclic electron flow. Chemosphere 93, 230–237.
829 https://doi.org/10.1016/j.chemosphere.2013.04.070
830 Wang, X., Feng, X., Zhuang, Y., Lu, J., Wang, Y., Gonçalves, R.J., Li, X., Lou, Y., Guan, W., 2019. Effects
831 of ocean acidification and solar ultraviolet radiation on physiology and toxicity of
832 dinoflagellate Karenia mikimotoi. Harmful Algae 81, 1–9.
833 https://doi.org/10.1016/j.hal.2018.11.013
834 Wieland, A., Kühl, M., McGowan, L., Fourçans, A., Duran, R., Caumette, P., Garcia de Oteyza, T.,
835 Grimalt, J.O., Solé, A., Diestra, E., Esteve, I., Herbert, R.A., 2003. Microbial Mats on the
836 Orkney Islands Revisited: Microenvironment and Microbial Community Composition. Microb.
837 Ecol. 46, 371–390. https://doi.org/10.1007/s00248-002-0108-2
838 Wootton, J.T., Pfister, C.A., Forester, J.D., 2008. Dynamic patterns and ecological impacts of declining
839 ocean pH in a high-resolution multi-year dataset. Proc. Natl. Acad. Sci. 105, 18848–18853.
840 https://doi.org/10.1073/pnas.0810079105
841 Yue, F., Gao, G., Ma, J., Wu, H., Li, X., Xu, J., 2019. Future CO2-induced seawater acidification
842 mediates the physiological performance of a green alga Ulva linza in different photoperiods.
843 PeerJ 7. https://doi.org/10.7717/peerj.7048

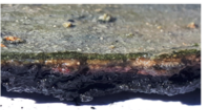

	Control 20°C – pH = 8	Acidification treatment 20°C – pH = 7.6	Warming treatment 24°C – pH = 8	Acidification + warming treatment 24°C – pH = 7.6
Photosynthetic efficiency	=	=	=	=
Extracellular polymeric substances	=	+ (bound carbohydrates EPS)	=	=
Chlorophyll a	=	-	=	=
Chlorophyll derivatives	=	+	=	=

Change in the phototrophic communities

OR

Change in the metabolism of green anoxygenic phototroph bacteria